Uncertainty Quantification in PEEC Method: A Physics-Informed Neural Networks-Based Polynomial Chaos Expansion

Yuan Ping, *Student Member, IEEE*, Yanming Zhang, *Member, IEEE*, and Lijun Jiang, *Fellow, IEEE*

***Abstract*—In this article, we propose a novel machine learning approach for uncertainty quantification (UQ) within the partial equivalent element circuit (PEEC) framework, employing physics-informed neural networks (PINNs)-based polynomial chaos expansion (PCE) scheme. Initially, the PEEC method is formulated via the electrical field integral equations and current continuity equations. Subsequently, random parameters are introduced to construct corresponding stochastic equations, thereby facilitating the generation of input–output data pairs for the training process. Then, by utilizing the PCE methodology, a mapping function is established. Next, the PINN-based approach is adopted to compute the coefficients of the polynomial bases, leveraging the matrix constructed from training data. Finally, this proposed approach enables the determination of stochastic parameters for quantities of interest within the PEEC method. The numerical examples involving the transmission lines are provided to verify the efficiency of the proposed method. It is found that the uncertainty is well quantified in each case. Compared to the traditional MCM, the proposed method can make UQ in the PEEC method 20 times faster. Hence, our work offers a practical machine learning approach for quantifying uncertainty, which could also be extended to other computational electromagnetic methods.**

***Index Terms*—Machine learning, partial equivalent element circuit (PEEC), physics-informed neural networks (PINNs), polynomial chaos expansion (PCE), uncertainty quantification (UQ).**

I. Introduction

THE partial element equivalent circuit (PEEC) method, originally proposed by Ruehli [1], has become a cornerstone in the field of electromagnetic (EM) simulation, offering a comprehensive 3-D full-wave modeling capability [2], [3]. This method is particularly lauded for its broad applicability, ranging from direct current to high-frequency scenarios, effectively capturing the EM behavior across the spectrum through the adept approximation of Green's function [4]. However, different random factors, such as constitutive [5], [6] and/or geometrical parameters [7], [8], are often induced by the inherent uncertainties during manufacturing processes of the electronic devices, which degrades the precision of the simulation in PEEC [9], [10]. Therefore, the adoption of uncertainty quantification (UQ) in the PEEC method is required for the stochastic modeling of the devices [11]. In particular, the effect of the current or field of interest is analyzed and the output quantity is then evaluated and statistically characterized [12]. Although other computational EM methods, such as the finite element method and finite differential time domain, can work in our method, they require absorbing and impedance boundary conditions. However, the PEEC method converts an EM problem into the circuit domain, the voltage or current source, and the circuit components, such as a resistor, capacitor, and resistor, are added into an equivalent circuit system by introducing extra current branches. Therefore, it is very convenient to realize excitation and load using the PEEC method. In addition, the voltages and currents of the ports can be obtained by directly solving the matrix equation (modified nodal analysis matrix). The S parameters can be obtained via the nodal current and voltage. The PEEC method is convenient to extract the port parameters by converting an EM problem into an equivalent circuit system. In addition, it provides an effective and straightforward approach to combining the EM problem with the circuit unit.

To this end, various methods have been proposed for the UQ issue, such as the Monte Carlo method (MCM) [13], stochastic Galerkin method (SGM) [14], stochastic collocation method (SCM) [15], etc. Herein, SGM is an intrusive method, where the terms in the deterministic equation that are affected by the uncertain terms are expanded by the polynomial chaos expansion (PCE) [14]. Galerkin testing is then used to form the stochastic matrix, which can become a large matrix that varies with the number of basis functions [16]. However, the number of functions increases with the number of random variables (RVs) and the highest order of polynomial bases [17], which could be prohibitive. The SCM is a nonintrusive method, where the collocation points can be obtained through different strategies. Specifically, SCM combines the high resolution of stochastic

Received 15 April 2024; revised 2 August 2024 and 23 August 2024; accepted 14 September 2024. Date of publication 1 October 2024; date of current version 18 December 2024. This work was supported in part by the Chinese University of Hong Kong Startup Fund under Grant 4937123, Grant 4937124, Grant 14223422, Grant 14201923, Grant 4937125, Grant 4937126, Grant 8601743 and Grant 4055185, in part by the Research Grants Council of Hong Kong under Grant GRF 14210623, in part by the ITF Grant ITP/007/23LP, in part by the AoE/E-101/23-N, and in part by the AoE/E-603/18. *(Corresponding author: Yanming Zhang.)*

Yuan Ping is with the Department of Electrical and Electronic Engineering, The University of Hong Kong, Pokfulam, Hong Kong, China (e-mail: yuanp019@connect.hku.hk).

Yanming Zhang is with the Department of Electronic Engineering, The Chinese University of Hong Kong, Satin, Hong Kong, China (e-mail: ymzhang@cuhk.edu.hk).

Lijun Jiang is with the Department of Electrical and Computer Engineering, Missouri University of Science and Technology, Rolla, MO 65409 USA (e-mail: ljf82@mst.edu).

Color versions of one or more figures in this article are available at https://doi.org/10.1109/TEMC.2024.3462940.

Digital Object Identifier 10.1109/TEMC.2024.3462940

Galerkin methods, which results from polynomial approximations in random spaces, with the ease of implementation of the MCM by sampling at discrete points in random spaces [18], [19]. However, all of these approaches are subject to the "curse of dimensionality" [20], [21]. Hence, it is still an open issue to develop a fast, accurate, and efficient method for the UQ problem.

Recently, the explosive growth of machine learning has ushered in a revolutionary wave of change across various electromagnetic compatibility (EMC) problems [22], [23], [24], particularly in addressing challenges that traditional methods struggle with [25]. Machine learning techniques are broadly categorized into supervised and unsupervised learning [26], [27]. Supervised learning, which requires labeled data, tends to consume substantial resources and suffers from limited portability [28]. On the other hand, unsupervised learning offers a rapid and straightforward approach [29], [30], presenting a promising pathway for solving UQ problems within the PEEC method.

In this article, we propose an unsupervised machine learning method, namely, a physics-informed neural networks (PINN)-based PCE scheme, for UQ problems in the PEEC method. First, the input and output observations employed as training data are obtained by introducing random parameters into deterministic PEEC equations to construct their corresponding stochastic form. Then, PCE is employed to construct the mapping function. Next, the PINN-based method is developed to calculate the coefficients of polynomial bases from the training data. Finally, the stochastic parameters of quantities of interest are obtained, and thereby the UQ is achieved in the PEEC method. Our contributions are listed as follows.

1) We develop a novel PINN-based PCE scheme for UQ in the PEEC method. As an unsupervised learning method, it employs the collocation method and PCE to construct the mapping function and polynomial matrix. Notably, it is not limited by the number of training data and can adapt to both overdetermined and underdetermined cases, when the proposed scheme is used to calculate the weights of the basis function in the UQ issues.
2) The proposed PINN-based approach combines the high-resolution capabilities of the SGM with the operational simplicity of Monte Carlo sampling techniques. This fusion not only enhances the computational efficiency by reducing the requisite number of samples, but also capitalizes on PCE to significantly refine the accuracy of the outcomes. Consequently, this scheme synergy offers a compelling advantage in the realm of the UQ, presenting a balanced blend of precision and practicality.
3) Our proposed PINN-based PCE method outperforms similar approaches, achieving over 20 times faster computation, highlighting its efficiency for the UQ problem in the PEEC method. Besides, the proposed machine learning scheme also could be extended to other computational EM methods in the future.

The rest of this article is organized as follows. The proposed PINN-based PCE method is detailed in Section II. The numerical examples are provided in Section III to verify the proposed method. Finally, Section IV concludes this article.

II. Methodology

In this section, we first introduce the PCE and PEEC methods. Then, the proposed PINN-PCE method for UQ in PEEC is detailed.

A. Polynomial Chaos Expansion

PCE, as a spectral method, illustrates the approximation of the input–output relationship by casting the model response onto orthogonal polynomials. Without loss of generality, the quantity of interest $\boldsymbol{Y}$ admits the spectral representation as follows:

$$\boldsymbol{Y}(\boldsymbol{\xi}) = \sum_{\alpha=1}^{K} y_\alpha \Psi_\alpha(\xi) \tag{1}$$

where Ψ_α denotes the polynomial basis, and y_α is the corresponding coefficient. Herein, the bases vary with different input RV distributions. Often, the RVs could be satisfied with specific functions, such as Gaussian, uniform, Gamma, and Beta distribution [31]. In particular, the space integrable functions with respect to the probability measure f_X admits a basis Ψ_α of polynomials orthonormal to each other, such that

$$\langle \Psi_\alpha(\xi), \Psi_\beta(\xi) \rangle = \int_{-\infty}^{\infty} \Psi_\alpha(\xi)\Psi_\beta(\xi) f_X(\xi) d\xi = \delta_{\alpha\beta}. \tag{2}$$

Here, $\delta_{\alpha\beta}$ is the Kronecker delta symbol, and K means the number of orthogonal polynomial bases, which could be determined by

$$K = \frac{(n+p)!}{n!p!} \tag{3}$$

where n is the number of RVs and p is the highest polynomial order. Obviously, the number of polynomial bases varies with the number of RVs and the highest order of polynomial bases. To be specific, the computational cost grows fast as the number of RVs or the highest order of polynomial bases increases. If the coefficients of the orthogonal polynomial bases are obtained, then the stochastic properties can be acquired subsequently. The mean value and variance of the quantity of interest, namely, $\mathbf{Y}(\xi) = \sum_{\alpha=1}^{K} u_\alpha \Psi_\alpha(\xi)$, are calculated as follows:

$$E\left(\mathbf{Y}(\xi)\right) = u_1 \tag{4}$$

$$Var\left(\mathbf{Y}(\xi)\right) = \sum_{\alpha=2}^{K} u_\alpha^2 \tag{5}$$

where u_α denotes the coefficient of αth orthogonal basis function.

B. PEEC Method

The PEEC method is derived from the electrical field integral equation (EFIE) and continuity equation, which is written as

$$\boldsymbol{E}_0(\boldsymbol{r}) = \frac{\boldsymbol{J}(\boldsymbol{r})}{\sigma} + j\omega \boldsymbol{A}(\boldsymbol{r}) + \nabla \boldsymbol{\phi} \tag{6}$$

and

$$\nabla \cdot \boldsymbol{J} = -j\omega\rho \tag{7}$$

where $\boldsymbol{E}_0$ means an applied electric field and $\boldsymbol{J}$ refers to the current density in the conductor with conductivity σ. $\boldsymbol{A}$ and ϕ are vector and scalar potential, respectively. ρ is the charge density. $\boldsymbol{r}$ represents the location of the observation location.

Then, using Green's function and space discretization, parasitic parameters in PEEC could be calculated as equivalent circuit elements. Next, these equivalent circuit elements form a densely coupled circuit network, where the modified nodal analysis in matrix form can be illustrated as

$$\begin{bmatrix} j\omega\mathbf{C}_p & \mathbf{A}_p \\ \mathbf{A}_p^T & -(j\omega\mathbf{L}_p + \mathbf{R}_p) \end{bmatrix} \begin{bmatrix} \mathbf{V} \\ \mathbf{I} \end{bmatrix} = \begin{bmatrix} \mathbf{I}_0 \\ \mathbf{V}_0 \end{bmatrix} \tag{8}$$

where $\mathbf{L}_p$ is a matrix representing all the inductive components including self-inductance and mutual inductance, and $\mathbf{C}_p$ is for the capacitance matrix. $\mathbf{R}_p$ is a diagonal matrix that contains resistors in inductive branches. The vectors $\mathbf{I}$ and $\mathbf{V}$ represent the branch currents and node voltages. $\mathbf{I}_0$ and $\mathbf{V}_0$ denote the current and voltage sources that are applied to the circuit system. $\mathbf{A}_p$ represents the connection matrix.

C. Proposed PINN-Based PCE in PEEC

In the following, we consider the input RVs, namely, $\xi(\xi_1, \ldots, \xi_n)$, in PEEC simulation. The corresponding output observations can be obtained, which is denoted as $\mathbf{Y}(y^1, y^2, \ldots, y^M)$. Herein, M represents the number of samples in the PEEC simulation, and n is the number of RVs. In particular, we use PCE to express Y as a polynomial function of ξ. Then, the relationship between $\xi(\xi_1, \ldots, \xi_n)$ and $\mathbf{Y}(y^1, y^2, \ldots, y^M)$ can be derived in a computationally efficient manner as follows:

$$\mathbf{Y}\left(y^1, y^2, \ldots, y^M\right) = \sum_{i=1}^{M} \sum_{\alpha=1}^{K} u_\alpha \Psi_\alpha\left(\xi^i\right) \tag{9}$$

where $\Psi_\alpha(\alpha = 1, 2, \ldots, K)$ denotes multidimensional orthogonal polynomial. u_α $(\alpha = 1, 2, \ldots K)$ means the coefficient of αth orthogonal basis function. It can be represented in the Vandermonde-type matrix form as follows:

$$\begin{bmatrix} \Psi_1\left(\xi^1\right) & \cdots & \Psi_K\left(\xi^1\right) \\ \vdots & & \vdots \\ \Psi_1\left(\xi^M\right) & \cdots & \Psi_K\left(\xi^M\right) \end{bmatrix} \cdot \begin{bmatrix} u_1 \\ \vdots \\ u_K \end{bmatrix} = \begin{bmatrix} y^1 \\ \vdots \\ y^M \end{bmatrix}. \tag{10}$$

Next, we establish the PINN to determine the coefficients of these orthogonal basis functions. Herein, the concept of PINN for both forward and inverse problems is first introduced by Raissi et al. [10], [12]. In [10] and [12], the differential equation is the governing equation with nonlinear parameters, and the variables of space or time domain are the input of the DNN to output the solution and nonlinear parameters. The outputs of the DNNs are employed to construct the differential equation by automatic differentiation. The loss function is the combination of the residual of the differential equation, boundary, and initial condition. In this work, we try to mimic the process of the PINN. The sample data of the QoI and the Vandemonde-type matrix are utilized to construct the loss function of PINN. Due to no boundary and initial condition, the residual of the matrix equation is only considered in the loss function. A set of random variables are regarded as the variables in the time or space domain, the stochastic parameters of the quantities of the interest, such as mean value and standard deviation, can be obtained by training the hyperparameters of the PINN. In our scenarios, the PINN method is explored to solve (10). The loss function of PINN is constructed with a sum of the mean squared errors as follows:

$$\boldsymbol{L} = \frac{1}{M} \sum_{i=1}^{M} \cdot \left(||\mathbf{B} \cdot \mathbf{U} - \mathbf{Y}||^2\right). \tag{11}$$

Herein, $B_{i\alpha} = \Psi_\alpha(\xi^i), \alpha = 1, \ldots, K, i = 1, \ldots, M$. Given the statistical model of the input and PCE model of the input–output map, the model response Y is not only known pointwise but can also be characterized statistically. For instance, the orthonormality of the polynomial basis ensures that the mean value and the variance of Y are derived as

$$E[Y] = u_1, \quad Var[Y] = \sum_{k=2}^{K} u_\alpha^2. \tag{12}$$

Fig. 1 illustrates the overall process of the proposed PINN-based method. The proposed method involves several steps. First, the PEEC function is determined by incorporating the EFIE and current continuity equation. Next, the modified analysis nodal matrix is obtained using Green's function and space discretization. The matrix of MNA is constructed, and it can be denoted as the deterministic PEEC. The sampling data are generated by the distribution of the RVs $\xi(\xi_1, \xi_2, \ldots, \xi_N)$. Then, the sampling data of the RVs are introduced to the deterministic matrix to construct the stochastic PEEC. By solving the stochastic PEEC, the nodal voltages and branch currents can be obtained. Subsequently, the sample data of the S parameter $\mathbf{Y}(y^1, y^2, \ldots, y^M)$ can be calculated by the nodal voltages and branch currents. In PEC, the S parameter is expended by the polynomial chaos, and the RVs ξ are substituted into the orthogonal polynomial function to construct a Vandemonde-type matrix $\mathbf{B}$. Then, the sample data of S parameter $\mathbf{Y}$ and the Vandemonde-type matrix $\mathbf{B}$ are employed to construct the loss function of the PINN. A set of random variables is regarded as the input of PINN. The stochastic parameters, such as mean value and standard deviation, can be obtained through training the parameters of the PINN.

III. Results

In this section, we conduct two different numerical examples to verify the proposed method, namely, multisegment transmission line and power divider. The considered RVs are Gaussian distributions. Therefore, the Hermite chaos is exploited to construct the polynomial bases. For the case with one random variable, the highest order of the polynomial function is 9, and then, the number of the polynomial bases is 10. For the case with three random variables, the highest order of the polynomial function is 3, and the number of polynomial bases is 20. For two random variables, the highest order is 3, and the number of the polynomial chaos could be 10 computed by (3). In addition, the random variables are mutually independent. It is worth noting that the patch is modeled as a perfect conductor with negligible thickness compared to the wavelength, eliminating the need to

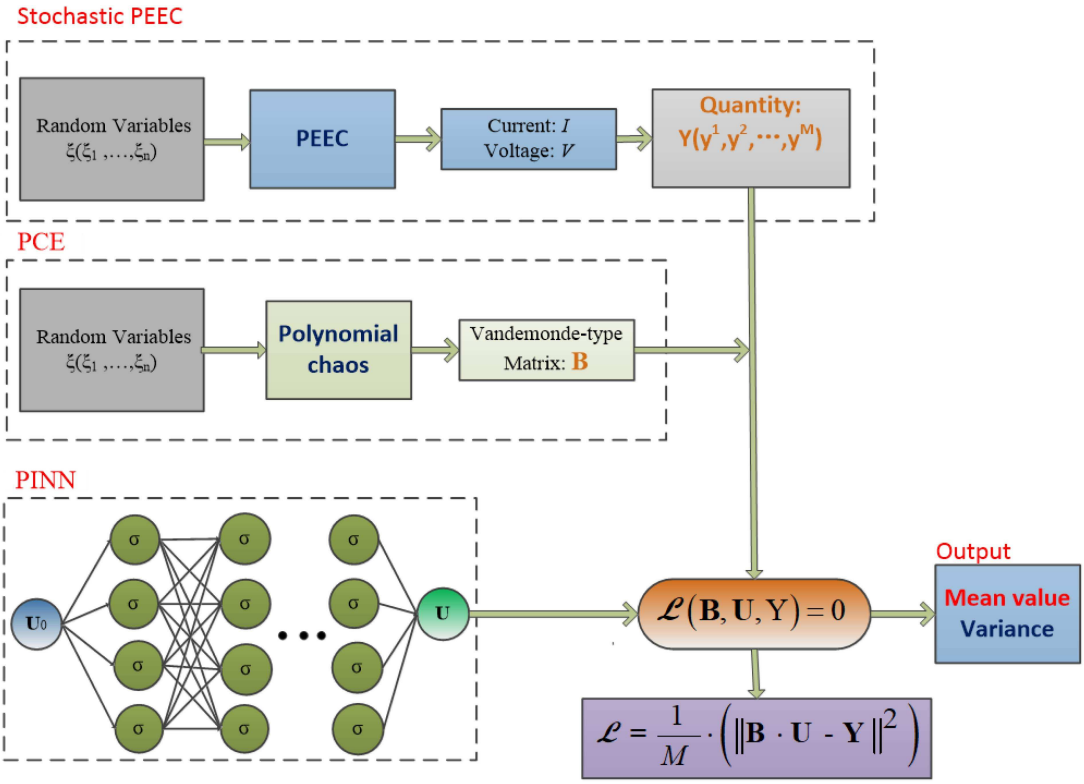

Fig. 1. PINN architecture for UQ problem in PEEC method.

consider skin depth. The metal part of the transmission line is considered as a plane. The material of the substrate is vacuum. All the results are compared with those of the conventional MCM to demonstrate the superiority of the proposed machine learning method. The sample data are from the PEEC simulation. The activation function of the DNN is tanh, Adam optimizer with learning rate 10^{-3} is employed to train the network.

The implementation of the PINN combing with PCE can be demonstrated as follows. Due to the S parameters considered in all the examples, the port voltages and the corresponding branch currents are considered the QoIs. The PEEC method is convenient for obtaining the parameters at the port. The nodal voltage is extracted at the given port and current at the additional branch is sampled. Then, the S parameter with random variables can be obtained. A set of random variables is regarded as the input of the PINN, and the coefficients of the polynomial are the output of the PINN. In our analysis, a third-order polynomial is utilized in the PCE analysis, necessitating 20 polynomial bases. The PEEC simulation employs 50 samples, while the PINN ascertains the polynomial base coefficients. Herein, the PINN is structured with four hidden layers, each comprising 40 neurons. The number of the training steps is 500. All the simulations are implemented at Intel Core i5-8500 CPU at 3.00 GHz within the MATLAB R2023b.

A. Case I: Multisegment Transmission Line

For the verification, we first consider a multisegment transmission line to examine the impact of multiple RVs on geometrical parameters using the proposed method. Fig. 2 illustrates two parallel transmission lines, identical in structure and dimensions,

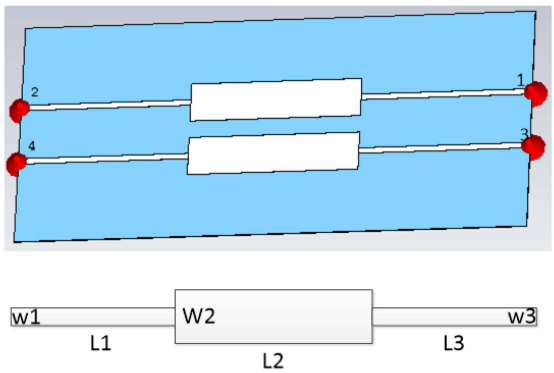

Fig. 2. Structure and the detail dimension of transmission line in Case I.

TABLE I
MEAN VALUE AND STANDARD DEVIATION OF RVS IN CASE I

	w1	w2	d
Mean value(mm)	1	6.915	10
Deviation	0.1	0.6195	1

with widths denoted as w1, w2, and w3 measuring 1, 6.915, and 1 mm, respectively. The lengths L1–L3 are uniformly 30 mm, while the interline center distance d stands at 10 mm. Ports 1–4 serve as impedance-matched excitation points. The lines are situated 0.2035 mm above the ground plane, and the geometrical parameters w1, w2, w3, and d could be considered as RVs. These results in three independent Gaussian-distributed RVs (w1 = w3) are detailed in Table I with their mean values and standard deviations.

TABLE II
COMPARISON RESULTS OF THE MEAN VALUE, STANDARD DEVIATION, AND TIME OF S11 CALCULATED BY THE MCM AND PINN-BASED METHOD AT 1 GHZ IN CASE I

	MCM	PINN	Relative error(%)
Mean value (dB)	-16.923	-16.869	0.32
Deviation	1.022	1.036	1.37
Time (s)	775.12	**48.29**	-
Speedup	-	**16**	-

The bold value denotes the computational time by the proposed method and the speedup of the proposed method compared with the Monte Carlo method. It is clear to illustrate the efficiency of the proposed method.

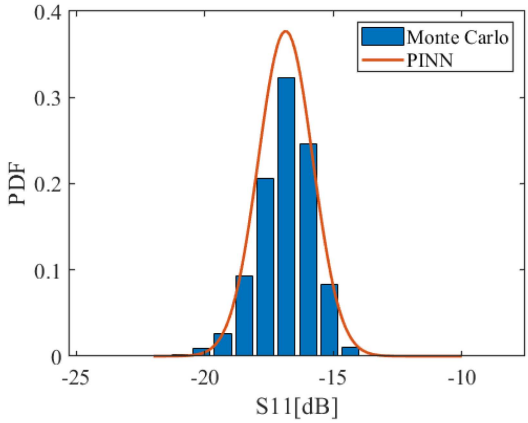

Fig. 3. Comparison of the probability density function of S11 calculated by the MCM and PINN-based method at 1 GHz in Case I.

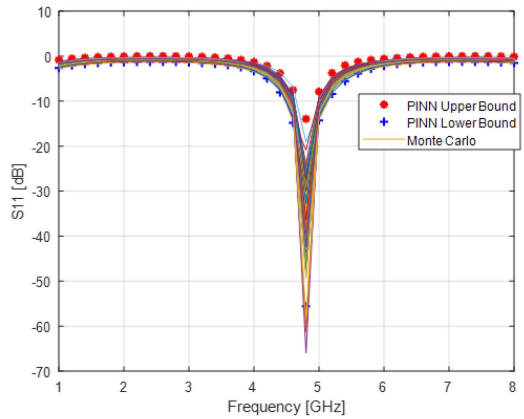

Fig. 4. Comparison result of upper and lower bound of S11 obtained by the MCM and PINN-based method in Case I.

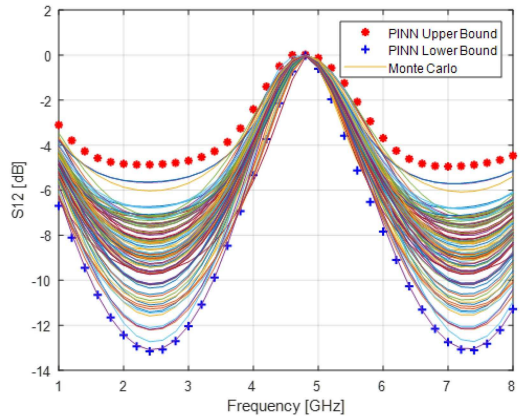

Fig. 5. Comparison result of upper and lower bound of S12 obtained by the MCM and PINN-based method in Case I.

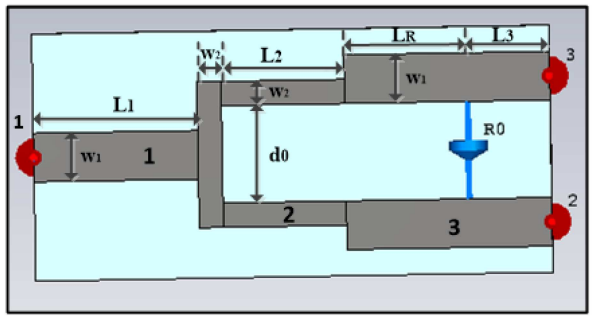

Fig. 6. Structure and the detail dimension of power divider in Case II.

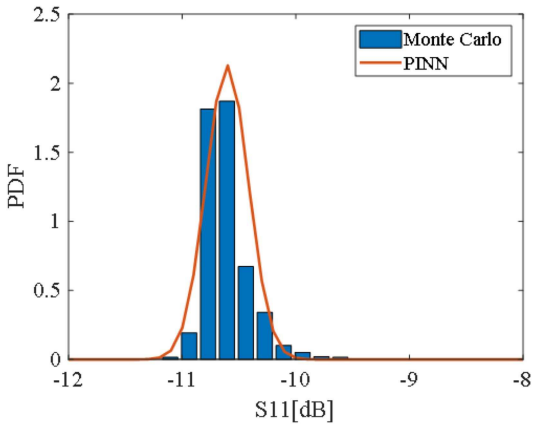

Fig. 7. Comparison of the probability density function of S11 calculated by the MCM and PINN-based method at 1 GHz in Case II.

To evaluate the performance of the proposed method, the stochastic parameters at single and multiple frequencies are analyzed. Also, the 10^3 sampling MCM results are used for the comparison. Table II presents the comparison results about the mean value and standard deviation of the S11 parameter at 1 GHz. It can be seen that the comparative analysis reveals relative errors in mean value and standard deviation of 0.32% and 1.37%, respectively. Fig. 3 plots the corresponding probability density function of the MCM and PINN. Clearly, a good agreement can be achieved in terms of the probability density function. Notably, time efficiency is also shown in Table II, with the PINN simulation concluding in 48.29 s, significantly outpacing the MCM's 775.12 s, thereby achieving a 16-fold speedup. All the comparison results are calculated on an Intel Core i5-8500 CPU at 3.00 GHz within the MATLAB R2023b. For further verification, we also test the S parameter across a 1–8 GHz frequency band, as shown in Figs. 4 and 5. The lower and upper bounds of the PINN-base method are calculated by $[u - 3\sigma, u + 3\sigma]$, compared with results from the MCM. The bounds of the PINN method agree well with those computed by the MCM method. Hence, we can conclude that the proposed PINN significantly enhances the efficiency and accuracy of the UQ of geometrical parameters in the PEEC.

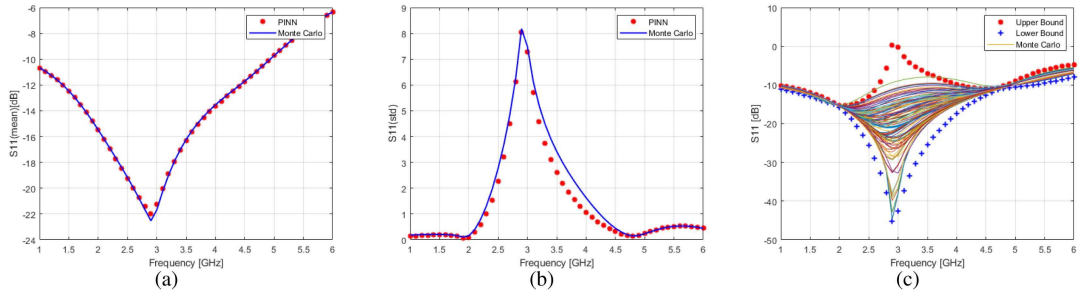

Fig. 8. Comparison results between the MCM and PINN with one RV condition in Case II. (a) Mean value. (b) Standard deviation. (c) Vounds.

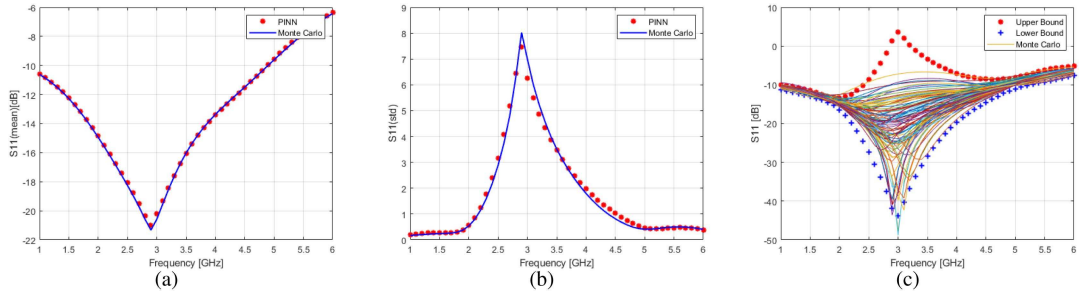

Fig. 9. Comparison results between the MCM and PINN with three RVs condition in Case II. (a) Mean value. (b) Standard deviation. (c) Bounds.

B. *Case II: Power Divider*

To further validate the proposed method, we consider another example of the power divider. Fig. 6 plots the structural and dimensional attributes of the model, which is characterized by its symmetry, with excitation ports denoted by red arrows and impedance-matched to 50 Ω. In particular, the power divider model is divided into three distinct parts, with the lengths of part 1, part 2, and part 3 being L_1, L_2, and $L_R + L_3$, respectively, assigned values of 20, 15, and 25 mm. Within part 3, L_R and L_3 have lengths of 15 and 10 mm, respectively. Also, the widths W_1 and W_2 are precisely 4.91 and 2.95 mm to achieve characteristic impedances of 50 Ω and 70.7 Ω, respectively. The distance between the ground plane is maintained at 1 mm. The spacing d_0 is defined as twice the width of W_1. The operational frequency is established at 5 GHz, and the connection resistor R_0 is valued at 100 Ω, thereby ensuring it is double the characteristic impedance of part 1.

Next, stochastic parameters at single and multiple frequencies are analyzed. The width of the transmission line affects its characteristic impedance, which in turn affects the performance of the S parameters. Therefore, three RVs, namely, W_1, W_2, and L_R, are considered. Herein, the polynomial of the highest order is 3 [see (3)] and thereby a total of 20 basis functions are used in PCE. Also, 50 sampling simulations of the PEEC are used to generate an orthogonal basis functions matrix. Accordingly, 20 random numbers are employed as inputs for the PINN. Besides, the PINN architecture with 4 hidden layers, each having 40 nodes, is designed, where the Adam optimizer is employed to update the network parameters.

Table III shows the stochastic parameters of three RVs. Through the analysis, the mean value and standard deviation of the S parameter at 1 GHz are presented in Table IV. Also, the MCM with 10^3 samples is calculated for the comparison. Clearly, the results obtained using the proposed method are in good agreement with those obtained from the MCM. The relative errors of the mean value and standard deviation are 0.0283% and 2.96%, respectively. In addition, the computational time required by the proposed method is more than twenty times less than that of the MCM. The workstation configuration is the same as the case I. Besides, the probability density function of MCM and PINN is depicted in Fig. 7. It can be seen that a good agreement can be obtained between these two methods.

TABLE III
MEAN VALUE AND STANDARD DEVIATION OF RVS IN THE POWER DIVIDER

	W_1	W_2	L_R
Mean value(mm)	4.91	2.95	15
Deviation	0.49	0.29	1.50

TABLE IV
COMPARISON RESULTS OF THE MEAN VALUE, STANDARD DEVIATION, AND TIME OF S11 CALCULATED BY THE MCM AND PINN-BASED METHOD AT 1 GHZ IN CASE II

	MCM	PINN	Relative error(%)
Mean value (dB)	-10.583	-10.586	0.028
Deviation	0.239	0.247	2.960
Time (s)	898.68	**42.18**	-
Speedup	-	**21**	-

The bold value denotes the computational time by the proposed method. and the speedup of the proposed method compared with the Monte Carlo method. It is clear to illustrate the efficiency of the proposed method.

For further demonstration of the performance of the stochastic parameters, the analysis of the S parameter with two conditions, namely, one RV and three RVs, are conducted, respectively. On the one hand, for one RV condition, we consider the W_1. Similarly, in this condition, we use the same PINN architecture with the single frequency scenario shown in Fig. 7. Through the proposed PINN-based method, we can obtain the mean value, standard deviation, and bounds, which are plotted in Fig. 8. Again, the MCM is applied to compute these statistical properties for the comparison. Obviously, the mean value, standard deviation, and bounds computed by the PINN align closely with those obtained from MCM's results.

On the other hand, we also consider the second condition with three RVs. The same PINN architecture is employed, and the MCM is also applied for the comparison. Fig. 9 shows the comparison results about the mean value, standard deviation, and bounds. We can see that a good agreement can be obtained between the MCM and the proposed PINN method. Hence, we can conclude that the proposed PINN-based method can realize UQ in PEEC with improved efficiency.

IV. Conclusion

In conclusion, we propose a machine learning-based approach utilizing PINN to address the UQ challenges in PEEC simulations. This PINN-based strategy adeptly handles stochastic matrices regardless of the dimensional relationship between rows and columns, effectively navigating the complexities inherent in regression-based methods. Through the integration of PCE, our approach reduces the requisite number of samples, thereby enhancing computational efficiency. The efficacy of our method has been demonstrated through the numerical examples, revealing that it outperforms existing methods with a computational speedup of about 20 times. Besides, the proposed approach holds the potential for extension to other computational EM frameworks, promising broader applicability for the UQ problem.

References

[1] A. E. Ruehli, "Inductance calculations in a complex integrated circuit environment," *IBM J. Res. Develop.*, vol. 16, no. 5, pp. 470–481, 1972.

[2] Y. S. Cao, Y. Wang, L. Jiang, A. E. Ruehli, J. Fan, and J. L. Drewniak, "Quantifying EMI: A methodology for determining and quantifying radiation for practical design guidelines," *IEEE Trans. Electromagn. Compat.*, vol. 59, no. 5, pp. 1424–1432, Oct. 2017.

[3] Y. S. Cao et al., "Inductance extraction for PCB prelayout power integrity using PMSR method," *IEEE Trans. Electromag. Compat.*, vol. 59, no. 4, pp. 1339–1346, Aug. 2017.

[4] A. Ruehli, G. Antonini, and L. Jiang, *Circuit Oriented Electromagnetic Modeling Using the PEEC Techniques*. Hoboken, NJ, USA: Wiley, 2017.

[5] M. Yusuf and S. Roy, "A polymorphic polynomial chaos formulation for mixed epistemic-aleatory uncertainty quantification of RF/microwave circuits," *IEEE Trans. Microw. Theory Techn.*, vol. 70, no. 1, pp. 926–937, Jan. 2022.

[6] A. K. Prasad and S. Roy, "Accurate reduced dimensional polynomial chaos for efficient uncertainty quantification of microwave/RF networks," *IEEE Trans. Microw. Theory Techn.*, vol. 65, no. 10, pp. 3697–3708, Oct. 2017.

[7] Y. Tao, F. Ferranti, and M. S. Nakhla, "Uncertainty quantification using parameter space partitioning," *IEEE Trans. Microw. Theory Techn.*, vol. 69, no. 4, pp. 2110–2119, Apr. 2021.

[8] M. Gossye, G.-J. Gordebeke, K. Y. Kapusuz, D. V. Ginste, and H. Rogier, "Uncertainty quantification of waveguide dispersion using sparse grid stochastic testing," *IEEE Trans. Microw. Theory Techn.*, vol. 68, no. 7, pp. 2485–2494, Jul. 2020.

[9] R. Torchio, L. Di Rienzo, and L. Codecasa, "Stochastic PEEC method based on polynomial chaos expansion," *IEEE Trans. Magn.*, vol. 55, no. 6, Jun. 2019, Art. no. 7204504.

[10] M. Raissi, P. Perdikaris, and G. E. Karniadakis, "Physics informed deep learning (Part I): Data-driven solutions of nonlinear partial differential equations," 2017, *arXiv:1711.10561*.

[11] A. F. Vincent, N. Locatelli, J.-O. Klein, W. S. Zhao, S. Galdin-Retailleau, and D. Querlioz, "Analytical macrospin modeling of the stochastic switching time of spin-transfer torque devices," *IEEE Trans. Electron Devices*, vol. 62, no. 1, pp. 164–170, Jan. 2015.

[12] M. Raissi, P. Perdikaris, and G. E. Karniadakis, "Physics informed deep learning (Part II): Data-driven discovery of nonlinear partial differential equations," 2017, *arXiv:1711.10566*.

[13] N. Metropolis and S. Ulam, "The Monte Carlo method," *J. Amer. Statist. Assoc.*, vol. 44, no. 247, pp. 335–341, 1949.

[14] R. G. Ghanem and P. D. Spanos, *Stochastic Finite Elements: A Spectral Approach*. Chelmsford, MA, USA: Courier Corporation, 2003.

[15] D. Xiu and J. S. Hesthaven, "High-order collocation methods for differential equations with random inputs," *SIAM. J. Sci. Comput.*, vol. 27, no. 3, pp. 1118–1139, 2005.

[16] K. Wu, H. Tang, and D. Xiu, "A stochastic Galerkin method for first-order quasilinear hyperbolic systems with uncertainty," *J. Comput. Phys.*, vol. 345, pp. 224–244, 2017.

[17] T. Sullivan, "Stochastic Galerkin methods," in *Introduction to Uncertainty Quantification*. Cham, Switzerland: Springer, 2015, pp. 251–276.

[18] A. Galetzka, D. Loukrezis, N. Georg, H. De Gersem, and U. Römer, "An HP-adaptive multi-element stochastic collocation method for surrogate modeling with information re-use," *Int. J. Numer. Methods Eng.*, vol. 124, no. 12, pp. 2902–2930, 2023.

[19] H. Miao et al., "Quantifying performance of passive systems in an integrated small modular reactor under uncertainties using multilevel flow modelling and stochastic collocation method," *Prog. Nucl. Energy*, vol. 149, 2022, Art. no. 104279.

[20] K. J. Gladwin and K. Vinoy, "An efficient SSFEM-POD scheme for wideband stochastic analysis of permittivity variations," *IEEE Trans. Antennas Propag.*, vol. 71, no. 2, pp. 1654–1661, Feb. 2022.

[21] M. Thapa, S. B. Mulani, A. Paudel, S. Gupta, and R. W. Walters, "Classifier-based adaptive polynomial chaos expansion for high-dimensional uncertainty quantification," *Comput. Methods Appl. Mech. Eng.*, vol. 422, 2024, Art. no. 116829.

[22] Y. Zhang and L. Jiang, "A novel data-driven analysis method for electromagnetic radiations based on dynamic mode decomposition," *IEEE Trans. Electromagn. Compat.*, vol. 62, no. 4, pp. 1443–1450, Aug. 2020.

[23] L. Jiang et al., "A novel physics-assisted genetic algorithm for decoupling capacitor optimization," *IEEE Trans. Microw. Theory Tech.*, vol. 72, no. 8, pp. 4498–4507, Aug. 2024.

[24] Y. Zhang and L. Jiang, "Space–time–frequency characterization in electromagnetic near-field scanning: A data-driven approach," *IEEE Trans. Electromagn. Compat.*, vol. 65, no. 6, pp. 1921–1929, Dec. 2023.

[25] R. Song, R. Xu, Z. Gu, and E.-P. Li, "Deep reinforcement learning-based pin map optimization of BGA package for EMC," in *Proc. Int. Appl. Comput. Electromagnetics Soc. Symp.*, 2023, pp. 01–03.

[26] L. Jiang, "Machine learning for EMC/SI/PI–blackbox, physics recovery, and decision making," *IEEE Electromagn. Compat. Mag.*, vol. 12, no. 4, pp. 65–75, Fourthquarter 2023.

[27] Y. Zhang, P. Ma, S. Gao, and L. Jiang, "An unsupervised learning framework for determining the excitation coefficients using near-field antenna measurements," *IEEE Trans. Electromagn. Compat.*, to be published, doi: 10.1109/TEMC.2024.3427682.

[28] H. Yao, Y. Zhang, L. Jiang, H. T. Ewe, and M. Ng, "Snow parameters inversion from passive microwave remote sensing measurements by deep convolutional neural networks," *Sensors*, vol. 22, no. 13, 2022, Art. no. 4769.

[29] Y. Zhang and L. Jiang, "Suppressing white-noise interference for orbital angular momentum waves via the forward–backward dynamic mode decomposition," *IEEE Trans. Antennas Propag.*, vol. 71, no. 3, pp. 2879–2884, Mar. 2023.

[30] G. James, D. Witten, T. Hastie, R. Tibshirani, and J. Taylor, "Unsupervised learning," in *An Introduction to Statistical Learning: With Applications in Python*. Cham, Switzerland: Springer, 2023, pp. 503–556.

[31] R. Askey and J. Wilson, "Some basic hypergeometric polynomials that generalize jacobi polynomials memoirs amer," *Math. Soc. AMS Providence RI 319*, 1985.